Soft Matter

PAPER

View Article Online
View Journal | View Issue

Cite this: *Soft Matter*, 2025, **21**, 8360

Line tension controls the spontaneous formation of vesicles

Anja F. Hörmann, [ab] Miriam Simon, [a] Christoph Brückner, [a] Sarah E. Rogers, [c] Lionel Porcar, [d] Ingo Hoffmann *[d] and Michael Gradzielski *[a]

Received 11th June 2025,
Accepted 17th October 2025

DOI: 10.1039/d5sm00600g

rsc.li/soft-matter-journal

Mixtures of the zwitterionic surfactant TDMAO and the anionic surfactant LiPFOS spontaneously self-assemble into well defined vesicles. The size of these vesicles is determined by the ratio of bending rigidity and line tension. By partially charging TDMAO, and thereby moving more to a catanionic system, the size of these vesicles can be controlled. Using stopped flow small angle neutron scattering we monitor the kinetics of vesicle formation and obtain their final size. Neutron spin echo spectroscopy allows for an independent measurement of the vesicle's bending rigidity. Combining this bending rigidity with the radius of newly formed vesicles, which is determined by the ratio of bending rigidity and line tension, we can determine the line tension. We find that it is the line tension that controls the trend in size of the vesicles. In summary, this means that here one has a surfactant mixture that delivers well-defined vesicles, whose size is controlled by the electrostatic interactions of the head groups.

1 Introduction

Spontaneous formation and thermodynamic stability of vesicles have been topics of scientific interest for a long time and especially thermodynamic stability has been debated intensively.[1–3] For a longer time vesicles were considered to be non-equilibrium bilayer structures of surfactants, until about 40 years ago some cases of spontaneous vesicle formation were reported.[4,5] In particular for oppositely charged surfactant mixtures spontaneous formation of small unilamellar vesicles by simple mixing of the surfactant solutions has been reported frequently, *e.g.* for the case of mixing dodecyltrimethylammonium bromide (DTAB) and sodium dodecyl sulfate (SDS),[6] other mixtures of sodium alkyl sulfates and alkyltrimethylammonium bromides,[7] cetyltrimethylammonium toluenesulfonate (CTAT) and the branched chain anionic surfactant sodium dodecylbenzenesulfonate (SDBS),[8] SDS and the double-chain cationic surfactant didodecyldimethylammonium bromide (DDAB),[9] cetyltrimethylammonium bromide (CTAB) and sodium perfluorooctanoate (FC7),[10] or the zwitterionic tetradecyldimethylamine oxide (TDMAO) and anionic dihydroperfluorooctanoic acid (DHPFOA), where the TDMAO under the chosen conditions was largely protonated.[11] The structures formed in such systems are likely determined by the bending energy, the spontaneous curvature and the line tension, as initially discussed for a mixture of CTAB and sodium perfluorooctanoate (FC7).[12] Spontaneous vesicle formation is not proof of their stability by itself. However, the facts that they often form over an extended period of time after having ceased any shear, meaning changes are purely due to diffusive transport of molecules, and that the vesicle size approaches a final value for minimum polydispersity indicate that an equilibrium situation, or at least a marked local thermodynamic minimum of free energy, has been achieved.[13] In addition, theoretical calculations have shown that one can expect formation of stable vesicles for mixtures of anionic and cationic surfactants for situations where one of the two surfactants is present in some excess,[14] and this is exactly what typically is observed experimentally.

While the formation of unilamellar vesicles in mixtures of cationic and anionic surfactants has been established rather generally,[15,16] their formation mechanism has remained a bit elusive, although it has been studied by means of the stopped-flow method and light scattering detection, for instance for the cases of mixing sodium dodecyl sulfate (SDS) and dodecyltrimethylammonium bromide (DTAB)[17] or cetyl trimethylammonium bromide (CTAB) with and sodium octyl sulfate (SOS) or dodecyl benzene sulfonic acid (HDBS).[18] From these experiments it was inferred that the formation process proceeds *via* initial formation of disk-like micelles that grow and then close to form unilamellar vesicles.[18] Similarly, the dissolution of catanionic vesicles by admixing cationic surfactant could well be monitored by stopped-flow experiments with turbidity detection.[19] However, from light scattering experiments one cannot deduce a refined structural picture and for many

[a] *Stranski-Laboratorium für Physikalische und Theoretische Chemie, Institut für Chemie, Technische Universität Berlin, Straße des 17. Juni 124, Sekr. TC 7, D-10623 Berlin, Germany. E-mail: michael.gradzielski@tu-berlin.de*
[b] *Bundesanstalt für Materialforschung und -prüfung (BAM), Unter den Eichen 87, D-12205 Berlin, Germany. E-mail: anja.hoermann@bam.de*
[c] *ISIS, Rutherford Appleton Laboratory, Harwell Oxford, Didcot OX11 0QX, UK*
[d] *Institut Max von Laue-Paul Langevin (ILL), F-38042 Grenoble Cedex 9, France. E-mail: hoffmann@ill.fr*

systems of interest the formation process occurs so quickly (faster than 1 ms) that it cannot be followed by stopped-flow experiments.[13,20]

In contrast to light scattering, small-angle neutron scattering (SANS) coupled to the stopped-flow technique does allow to observe the structural changes on the mesoscopic scale in detail, as demonstrated a longer while ago for the case of admixing salt to micellar AOT solutions, which led to the formation of unilamellar vesicles, whose formation and growth could be followed in thorough detail[21] and bending energy of the bilayer[22–25] Coming back to the case of mixed surfactant systems, a longer while ago, we had studied a system of a perfluorinated anionic surfactant mixed with the zwitterionic tetradecyldimethylamine oxide (TDMAO), which is directly related to catanionic systems as the TDMAO will be partly positively charged. Very interestingly by reducing the attractive interaction between the surfactant pair by exchanging the cationic surfactants by a zwitterionic surfactant one is able to slow down the formation process.[26] In this way the charge–charge interaction of the head groups is substituted by a charge–dipole interaction, which is much weaker[27] and correspondingly also the formation process is substantially slowed down in such mixtures. Accordingly, it was possible to monitor it well by time-resolved small-angle X-ray scattering (SAXS) experiments, as in this systems also the contrast conditions for SAXS experiments are good.[28] These experiments revealed that during the formation process first some small disks are formed that are growing in size until subsequently they close and transform to unilamellar vesicles. This pathway of vesicle formation is controlled by the balance of line tension (the energy penalty at the edges of the disks due to the high local curvature) and bending energy of the bilayer.[22–25]

Knowing this it was also possible to control size and time of the formation of such vesicles by addition of an amphiphilic copolymer that leads to a longer growth process and correspondingly larger vesicles.[29] This effect of the copolymer can be ascribed to a lowering of the line tension and is following the old concept of vesicle size control by employing ''edge-active agents''.[30] According to this mechanism, this kinetically controlled size of the vesicles should be given by[22]:

$$R_v = 2\frac{2\kappa + \bar{\kappa}}{\Lambda} \quad (1)$$

where κ and $\bar{\kappa}$ are the mean and the saddle-splay modulus of the bilayer, respectively, and Λ the line tension. (The equation is typically given as the maximum disk radius beyond which vesicles spontaneously form; by removing a factor of two this is equivalent to the radius of the vesicles that form by bending and closing of a single disk). Such experiments do not allow to differentiate between contributions from mean and saddle-splay modulus and in the remainder of this paper we will use the term bending rigidity as an averaged quantity containing contributions from both moduli.

As indicated, experiments regarding spontaneous vesicle formation were done extensively by us before, employing the zwitterionic surfactant tetradecylamine oxide (TDMAO) and perfluorinated anionic surfactants, where the latter is promoting formation of bilayers over an extended range of mixing ratios. However, in these experiments we always studied mixtures of anionic and zwitterionic surfactants, *i.e.* kept the interactions between the head groups constant. Now it was clearly interesting to interpolate between the too fast to observe formation process present for anionic/cationic surfactant mixtures to that of anionic/zwitterionic surfactant mixtures, in order to learn how the head group interactions precisely control this process. With increasing strength of the headgroup interactions we expect an increase in packing parameter[31] due to a reduction in preferred headgroup area, and therefore an increase in the penalty for forming the highly curved rim of the disks (Λ). On the other hand, a decrease in headgroup area should significantly stiffen the bilayer.[32] Fortunately, for the surfactant TDMAO a change in headgroup properties is rather easy as its protonated version has about the acidity of acetic acid ($pK_a \sim 5$[33]). We can therefore protonate TDMAO by simply lowering the pH of the solution using a strong acid.

To study vesicle formation as a function of the head group interactions we therefore did time-resolved stopped-flow SANS experiments in which we mixed lithium perfluorooctanesulfonate (LiPFOS) with TDMAO that was protonated to a given extent by HCl. In addition, the Pluronic L35 was present in the mixtures in order to slow down the formation process.[29] By analysis of the time-resolved SANS spectra we were able to discern the temporal structural evolution resulting in vesicle formation with a main parameter being the final vesicle size. This allows to interpret the systems in terms of bending elasticity and line tension (eqn (1)). Neutron spin echo spectroscopy (NSE) performed on identical samples yields an independent estimate of the bending modulus of the bilayer. This completes the picture on how bending moduli and line tension vary with the head group interactions from a zwitanionic toward a catanionic surfactant mixture.

2 Materials and methods

2.1 Materials

Tetradecyldimethylammonium oxide (TDMAO, $C_{14}H_{29}(CH_3)_2NO$) was obtained free of charge from Stepan (Stepan Company, Northfield, Illinois, USA) as Ammonyx M solution and used after freeze-drying without further purification. Lithium perfluorooctylsulfonate (LiPFOS, $C_8F_{17}SO_3Li$, >96%) was purchased from TCI Europe and used without further purification. Pluronic L35 ($EO_{11}PO_{16}EO_{11}$, L35) was received as a gift from BASF (BASF SE, Ludwigshafen, Germany) and used without further purification. Deuterium chloride (DCl) was purchased from Sigma Aldrich (Merck, Burlington, Massachusetts, USA) as 35% (w/w) solution in D_2O. Deuterium oxide (D_2O, 99.9%) was obtained from deutero and filtrated using a cellulose acetate (CA) filter of 0.45 μm pore size.

Target composition of samples was 50 mM total surfactant concentration with a molar fraction of 55% TDMAO, where the TDMAO is protonated to a degree X and has 1%(n/n) L35

added. For transparency, we give the actual compositions based on weights here. We prepared stock solutions of (TDMAO + 1.04%(n/n) L35), 300 mM, LiPFOS, 405 mM and DCl, 199 mM in D_2O for further dilution on the site of the experiment. From these stocks we prepared at ISIS: one solution of (TDMAO + 1%(n/n) L35), 97 mM, one dilute DCl solution, 98 mM, and three LiPFOS solutions, 52.5(3) mM. Mixing of these solutions in the stopped-flow apparatus is described in subsection Section 2.2. For static measurements (SANS and NSE) the same stock solutions were diluted again, yielding concentrations of 101 mM for the TDMAO/L35 mixture, 100 mM for DCl, and 47.1 mM for LiPFOS. The mixing sequence both for static and stopped-flow experiments was chosen to let the last addition, LiPFOS solution, meet a pre-charged (TDMAO + L35) solution at the same target concentration of 50 mM. For this purpose, the TDMAO stock was first mixed with the DCl solution and then diluted with D_2O. For static measurements, LiPFOS solution was added at least 75 minutes after preparation of the charged TDMAO solution. The resulting samples had a TDMAO fraction of 57.0(3)% and surfactant concentration 49.0(2) mM, with actual charge ratios 0.97 times target values. To compare, during stopped-flow experiments a TDMAO fraction of 53.0(1)% at 50.3(1) mM surfactant concentration was obtained and charge ratios were 0.99 times target values. Comparability of samples can safely be assumed based on this data thanks to the well-characterized phase diagram of the TDMAO/LiPFOS system.[25,34]

2.2. Methods

SANS was carried out on the Sans2d small-angle diffractometer at the ISIS Pulsed Neutron Source (STFC Rutherford Appleton Laboratory, Didcot, U.K.).[35,36] A simultaneous range of the magnitude of the scattering vector q ($q = 4\pi/\lambda \sin(\theta/2)$, with neutron wavelength λ and scattering angle θ) of 0.042–7.21 nm^{-1} was achieved utilising an incident wavelength range of 1.75–16.5 Å and employing a sample to detector distance of 4 m, with the 1 m^2 detector offset vertically 60 mm and sideways 100 mm. Each raw scattering data set was corrected for the detector efficiencies, sample transmission, and background scattering from the empty cell and converted to absolute scale with a standard sample (a solid blend of hydrogenous and perdeuterated polystyrene) using the software Mantid.[37]

A stopped flow apparatus (BioLogic SFM-400) was employed to mix the surfactant solutions. The four reservoirs were employed to first mix a 100 mM TDMAO solution containing the desired concentration of L35 with the appropriate quantity of 100 mM DCl solution to achieve the degree of protonation X of TDMAO. The result was then diluted to a TDMAO concentration of 50 mM. Finally, 50 mM LiPFOS solution was added in a volumetric ratio of 45 : 55. The flow rate was fixed at 2 mL s^{-1}. The mixing volume was 600 μL. The kinetics were recorded for at least 2 minutes.

Additional static SANS measurements were performed on the instrument D22 at Institut Laue-Langevin (ILL, Grenoble, France). Samples were measured at three configurations: sample-to-detector distance 1.5 m using a collimation of 2.8 m and wavelength 6.0 Å, sample-to-detector distance 8 m using a collimation of 8 m and wavelength 6.0 Å, and sample-to-detector distance 17.6 m using a collimation of 17.6 m and wavelength 12.0 Å. After an initial sequence of measurements for a set of samples (from high to low q) several measurements at low q were done to check for further changes in vesicle size. Detector efficiency, sample transmission and background corrections were performed using LAMP[38] with water as a secondary standard for absolute scale. Data at low q were corrected using water measured in the 8 m configuration and scaled using the appropriate correction factor[39] before merging and rebinning using dataMerge.[40] Unless stated differently, SANS measurements are from Sans2d.

The coherent scattering intensity of an isotropic ensemble of non-interacting particles which are polydisperse in a dimension R is given by

$$I(q) = {}^1N \int_0^\infty g(q) \int_0^\infty f(R) P(q,R) \mathrm{d}R \mathrm{d}q, \quad (2)$$

where ${}^1N = \varphi / \int_0^\infty f(R) V(R) \mathrm{d}R$ is the particle number density with the particle volume fraction ϕ, the size distribution function $f(R)$ and the particle Volume $V(R)$. $P(q,R)$ is the particle form factor and $g(q)$ is the width of the distribution in q due to the resolution of the instrument. Vesicles can be modelled as spherical shells. Their form factor is given by

$$P_{\mathrm{ves}}(q) = \left(\sum_{i=0}^{1} \frac{4\pi R_i^3}{3} \Delta\mathrm{SLD}_i \frac{3(\sin(qR_i) - qR_i \cos(qR_i))}{(qR_i)^3} \right)^2, \quad (3)$$

where R_0 is the inner radius and R_1 is the outer radius so that the shell thickness is $d_s = R_1 - R_0$ and $\Delta\mathrm{SLD}_i$ is the difference in scattering length density going from $R > R_i$ to $R < R_i$. The form factor of a disk is given by

$$P_{\mathrm{disk}}(q) = \int_0^1 \left(\pi r^2 L \Delta\mathrm{SLD} \frac{2J_1\left(qr\sqrt{1-x^2}\right)}{qr\sqrt{1-x^2}} \frac{\sin(qLx/2)}{qLx/2} \right)^2 \mathrm{d}x, \quad (4)$$

with first order Bessel function J_1, the radius of the disk r, its thickness L and the difference in scattering length density between the disk and the surrounding solvent. The data were described as a sum of vesicles and disks so that the overall volume fraction ϕ is related to the volume fraction of vesicles by $\phi_{\mathrm{ves}} = x_{\mathrm{ves}}\phi$ and the volume fraction of disks by $\phi_{\mathrm{disk}} = (1 - x_{\mathrm{ves}})\phi$.

The distribution of radii of both vesicles and disks is described with a log-normal distribution

$$f(r') = \frac{1}{\sqrt{2\pi}\sigma \cdot r'} \exp\left(-\frac{(\ln(r') - \mu)^2}{2\sigma^2} \right). \quad (5)$$

where $r' = R/r_0$ and $r_0 = 1$ nm. The mean value of the distribution reads $R_{\mathrm{mean}} = \exp(\mu + 1/2\sigma^2) \cdot r_0$, the standard deviation is $\mathrm{SD} = \sqrt{(\exp(\sigma^2) - 1)} \exp(\mu + 1/2\sigma^2) \cdot r_0$ and the relative standard deviation $\mathrm{SD}/R_{\mathrm{mean}}$ was fixed at 15% for the disks and used as a fit parameter for the vesicles.

The distribution in q, $g(q)$ is given by a Gaussian with a q dependent standard deviation, which is given by the instrumental resolution.

In practice, the size and polydispersity of the vesicles were determined from the last curve of a stopped flow measurement, assuming that there are only vesicles. To obtain fits where the depth of both the first and second form factor oscillation is accurately described, it was necessary to assume that there is a small fraction of vesicles which result from the fusion of two disks instead of the deformation and closure of a single disk. While in principle disk fusion may occur at any time during disk growth, for the sake of simplicity, we assume that the vesicles resulting from fusion have twice the surfactant volume of the smaller vesicles. For the remainder of the article we will refer to the smaller vesicles simply as vesicles and quantities like vesicle radius refer to those smaller vesicles unless otherwise specified since their mechanism of formation is the subject of this study. With these size parameters of the vesicles fixed, the time series was fitted with the disk radius and the fraction of disks as free fit parameters, while the thickness of the bilayers, both in disks and vesicles was fixed at 2.8 nm based on previous results.[34] Determining the size and number of vesicles relative to the number of disks relies on the determination of the position and depth of the form factor minima. The large vesicles are necessary to adjust the ratio between the depth of the first and second form factor minimum. The effect of disk-like micelles, smaller vesicles and larger vesicles on the SANS model is shown in Fig. S1.

NSE measurements were performed on the instrument IN15 at ILL.[41] Samples were measured at a neutron wavelength of 10 Å and detector angles of 4.5° and 7.5° reaching a maximum Fourier time t of 194 ns and covering a q range from 0.39 to 0.931nm^{-1}. Selected samples were also measured at 17 Å, 3° and 13.5 Å, 3.5° extending the Fourier time range to 952 and 477 ns, respectively and extending the q-range at low q down to 0.14 1 nm^{-1}. NSE directly yields the intermediate scattering function $S(q,t)$. In the framework of the classical Zilman–Granek theory for large, flat, thin membranes $S(q,t)$ follows a simple stretched exponential.[42] An extended version of the theory that takes into account finite size effects in spherical geometry and translational diffusion has been published recently.[43] In short, $S(q,t)$ is given by

$$S(q,t) = \left\langle P(q) \exp\left(-\frac{q^2 R^2 \langle \Delta u^2(t) \rangle}{2}\right) \exp\left(-D(R) q^2 t\right) \right\rangle, \quad (6)$$

where the angular brackets indicate an average over the vesicle size. $D(R)$ is the translational diffusion coefficient which depends on the vesicle radius through the Stokes–Einstein equation $D = \frac{k_B T}{6\pi\eta R}$, with Boltzmann constant k_B, temperature T and solvent viscosity η. For the size, we use values obtained from SANS but results from IN15's online dynamic light scattering setup are in reasonable agreement (see Fig. S13). For the form factor of the vesicle $P(q)$ we use the approximation for a thin spherical shell. The mean square displacement $\langle \Delta u^2(t) \rangle$ is given by

$$\langle \Delta u^2(t) \rangle = \frac{1}{2\pi} \sum_{l=2}^{l_{max}} (2l+1) \left\langle |u_l|^2 \right\rangle (1 - \exp(-\omega_l t)), \quad (7)$$

with the relaxation rate of mode l

$$\omega_l = \frac{\kappa}{\eta R^3} \frac{(l-1)l(l+1)(l+2)(l(l+1))}{4l^3 + 6l^2 - 1} \quad (8)$$

and its mean square amplitude

$$\left\langle |u_l|^2 \right\rangle = \frac{k_B T}{\kappa} \frac{1}{(l+2)(l-1)(l(l+1))}. \quad (9)$$

A simple back of the envelope calculation shows that for such small vesicles, taking into account the diffusion term is important. The diffusion coefficient of a 20 nm radius vesicle at room temperature in heavy water is about 1 Å^2 ns^{-1}. At a q value of 0.5 nm^{-1} (roughly in the middle of our q range) and after 200 ns (our maximum Fourier time) diffusion alone causes a decay of $S(q,t)$ down to 0.6 without any contribution from membrane undulations. The time and length scales observed by NSE are such that in its high q limit the observed bending rigidity corresponds to the unrelaxed bending rigidity $\bar{\kappa}$ rather than the relaxed bending rigidity κ.[44] Both bending rigidities are related by $\bar{\kappa} = \kappa + 24(d/d_{bilayer})^2$[45,46] where $d_{bilayer}$ is the (hydrophobic) bilayer thickness and d is the height of the neutral surface, which is not precisely known. While the transition becomes visible at lower q, it has proven challenging to extract reliable values of κ and the values reported here are those obtained in the indicated q range, which corresponds to the unrelaxed bending rigidity $\bar{\kappa}$ in the high q limit. The unrelaxed bending rigidity is generally found to be about an order of magnitude larger than the relaxed bending rigidity.[47,48]

3. Results and discussion

To elucidate both the structure and the kinetics of formation of the vesicles, we performed sf-SANS measurements. The last SANS curve of each time series was used to determine the size and polydispersity of the vesicles.

Previously, it has been shown that mixing micellar solutions of TDMAO and LiPFOS leads to the formation of vesicles.[25,29] Mixing the two surfactants, leads to the formation of disklike micelles. These disklike micelles, through their bending undulations close on themselves to form vesicles. By forming vesicles, they can release the extra free energy from their rim at the expanse of an increased bending energy. Therefore, the size of the vesicles is determined by the ratio of bending energy and line tension according to eqn:rves. The formation and growth of disks in this system is finished after a few seconds and here, with a shortest time of 2.5 s we mostly observe the formation of vesicles from disks.

The scattering curves show the typical scattering pattern of relatively monodisperse vesicles with a plateau at low q,

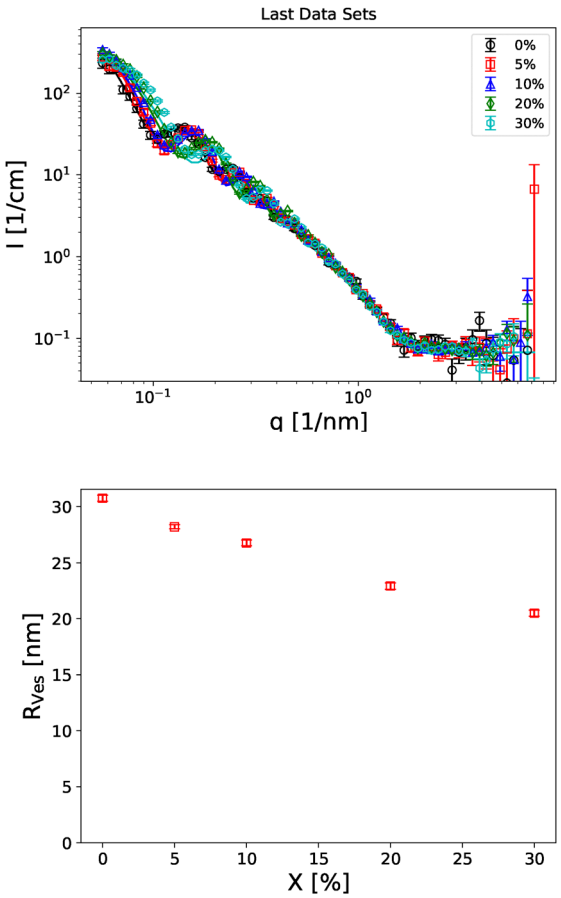

Fig. 1 Top: SANS curves of readily formed TDMAO/LiPFOS vesicles with 1% L35. The shape of the scattering patterns indicates the formation of vesicles and the shift of the first form factor minimum towards higher q with increasing fraction of charged TDMAO indicates the formation of smaller vesicles. Bottom: Inner radii of TDMAO/LiPFOS vesicles as a function of the fraction X of charged TDMAO for samples with 1% of L35 as obtained from the last SANS curve of sf-SANS measurements; The size of the vesicles decreases with increasing X. Parameter errors for the inner radius are small thanks to the well-defined form factor minima and fixed shell thickness.

followed by form factor oscillations and a slope $I \sim q^{-2}$. An increased fraction of charged TDMAO and therefore fewer charges on the membrane leads to smaller vesicles as indicated by the shift of the leftmost form factor oscillation to higher q (see Fig. 1, top and Fig. S2). The obtained radii are summarised in Fig. 1 (bottom). Parameter error estimates for the radii are small since the vesicle form factor oscillations are well-defined (see Fig. 1 (top)) and the thickness is fixed based on previous results[34] as stated above. By charging 30% of the TDMAO the radius decreases by about 10 nm from 30 to 20 nm. The polydispersity, expressed as the relative standard deviation of the vesicles remains roughly constant (see Fig. S3) with the fraction of charged TDMAO.

While it helps to improve the quality of the fits, the fraction of larger vesicles with twice the surfactant volume does not show a systematic trend (see Fig. S4). Omitting the fraction of larger vesicles leads to discrepancies between fit and data near the first form factor minimum but does not seriously affect the fit parameters (see Fig. S5). It is tempting to attribute this behaviour to deformations of the spherical shape of the vesicles due to the undulation motions. However, using eqn (6) and (7) with $\kappa = 20\ k_BT$, 30 nm vesicle radius and omitting diffusion results in values of $S(q,\infty)/S(q,0)$ of 0.99 and 0.95 at $q = 0.1$ and 0.2 nm^{-1}, the positions of the first two formfactor minima. It is therefore safe to assume that the undulations have a minor influence at these low q values.

Fixing the parameters of the vesicles and leaving the fraction of vesicles and the size of the disks as free parameters, we can monitor the formation of vesicles (see Fig. 2, (top) as much as Fig. S6–S8 for the fits). The data can be reasonably described with a simple exponential $1-x_{Ves} = a\cdot\exp(-t/\tau)$ where the amplitude a is free between 0.9 and 1.1 and τ is the characteristic time of vesicle formation (see Fig. 2, bottom). Measurements of independently prepared samples with the same composition, several hours after mixing them, show good agreement with the data from sf-SANS (see Fig. S9 and S10). Decreasing the charge of the membrane by protonating the TDMAO obviously accelerates the process of vesicle formation.

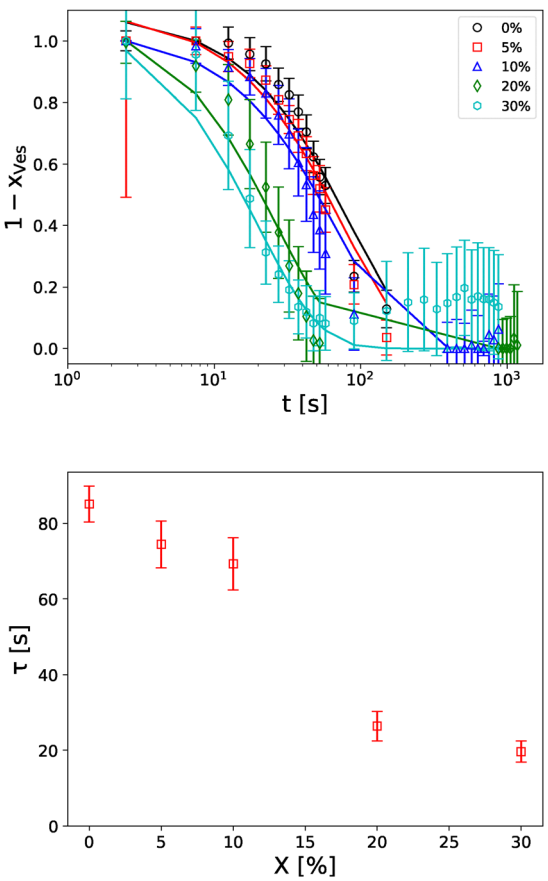

Fig. 2 Top: 1-Fraction of vesicles as a function of time from sf-SANS measurements for different fractions of charged TDMAO X for 1% of L35 with exponential fits. The formation of vesicles is faster with higher values of X. Bottom: Characteristic time of vesicle formation as function of X for samples with 1% L35. The characteristic time τ decreases with X.

In the long time limit, x_{ves} tends to 1, within error, which underlines that the fits are physically meaningful. For the shortest times, x_{ves} tends to 0, which means that the time resolution of the sf-SANS experiment is sufficient to monitor the whole process of vesicle formation. Increasing the fraction X of charged TDMAO leads to an accelerated formation of vesicles. Looking at the evolution of the disk radii, it can be seen that in the time frame of the experiment, their size grows only slightly, which is in agreement with previous results, where it was shown that the disk growth is finished after about 1 s.[25] For longer times the error bars for the disk radius become large and the values are erratic since the fraction of disks becomes very small (see Fig. S11).

As the final size is determined by the ratio of bending rigidity and line tension (see eqn (1)), we can combine the radii of the vesicles obtained by SANS with values of the bending rigidity from NSE to calculate the line tension.

Applying eqn (6) with κ as the only free parameter, the values shown in Fig. 3 are obtained (see Fig. S12 for the fits).

Interestingly, even for the very small vesicles investigated here, κ only becomes constant above roughly 0.6 nm^{-1} and this does not seem to depend on the size of the vesicles, as the same observation was made for significantly larger phospholipid vesicles with a radius of up to 100 nm.[43] Therefore, a global fit of only the spectra with $q > 0.6$ nm^{-1} was performed, which yields the bending rigidities presented in Fig. 4. These values show an increase with X. Whether or not the fraction of large vesicles is taken into account in the fits has hardly any influence on the obtained value of the bending rigidity. The fact that the vesicles become smaller, even though the bending rigidity increases with X means that the trend in the bending rigidity must be overcompensated by the line tension.

Combining results from SANS and NSE to calculate the line tension, the values shown in Fig. 5 are obtained and necessarily show an increase with increasing X. The values are in a similar range as those determined from the kinetics of the closure of pores in DOPC giant unilamellar vesicles.[49] This raises the interesting question, whether the relevant bending rigidity for the closure of the disks is the unrelaxed bending rigidity as determined by NSE in its high q limit or the relaxed bending rigidity which would be roughly an order of magnitude lower. In that sense, the values of the line tension obtained here, should be regarded as an upper limit.

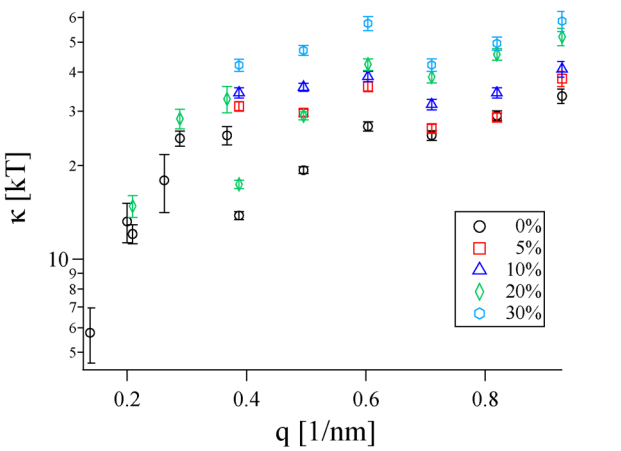

Fig. 3 Bending rigidity κ obtained from NSE through eqn (6) as a function of q for samples with 1% L35. The values are stable above $q \sim 0.6$ nm^{-1} and increase with X.

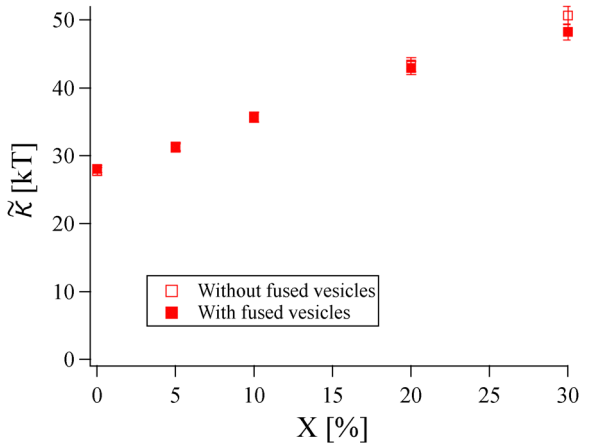

Fig. 4 Unrelaxed bending rigidity obtained from NSE using eqn (6) for $q > 0.6$ nm^{-1}. The value of $\tilde{\kappa}$ increases with X.

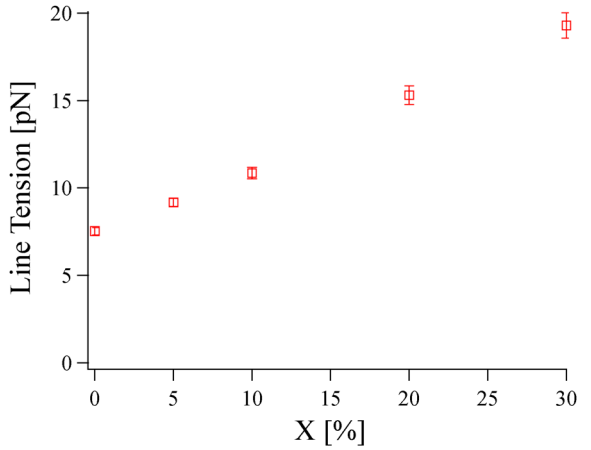

Fig. 5 Line tension obtained from combining $\tilde{\kappa}$ from NSE and R_{ves} from SANS measurements. An increase in Λ with X is observed.

The observed trend in the line tension can be rationalised with a simple packing parameter argument.[31] Karatekin *et al.*[49] observed that adding molecules with a small packing parameter (large headgroup with a thin chain, lysolipid in their case) stabilises the rim while adding molecules with a larger packing parameter (small headgroup, bulky chain, cholesterol in their case) destabilises the rim. It has been observed previously[27] that the neutral couple TDMAOH/LiPFOS yields a larger packing parameter than TDMAO/LiPFOS and therefore destabilises the rim, leading to a faster formation of smaller vesicles.

Conclusions

In summary, we performed sf-SANS and NSE measurements on mixtures of zwitterionic TDMAO and anionic LiPFOS with 1 wt%

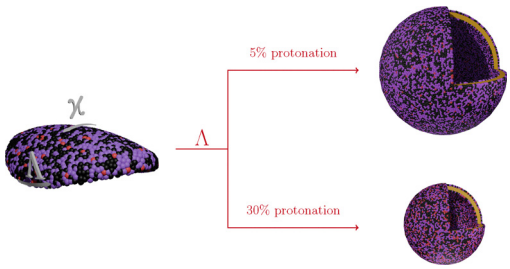

Fig. 6 The size of vesicles formed from disklike micelles is determined by the ratio of bending rigidity and line tension (see eqn (1)). Protonating the headgroup of TDMAO and thereby reducing the overall charge of the vesicle membrane leads to a decrease in vesicle radius due to an increase in line tension.

Pluronic L35 which are forming vesicles. The kinetics of formation from disklike micelles to vesicles can be monitored using sf-SANS while NSE gives an independent measure of the bending rigidity of the vesicles. As the size is determined by the ratio of bending rigidity and line tension, combining the size from SANS and the bending rigidity from NSE allows to determine the line tension. The vesicles become smaller with an increased fraction of charged TDMAO which reduces the overall charge of the membrane (see Fig. 6). This seems counterintuitive at first since a reduction of charge in the membrane should lead to a smaller headgroup area, which should reduce the spontaneous curvature, which in turn should favour larger vesicles. NSE measurements show that the bending rigidity increases, which should also favour larger vesicles. Therefore, the decrease in size must be controlled by the line tension.

With the line tension as the decisive factor, the trend of vesicle size with membrane charge is readily understood. A larger packing parameter increases the line tension, which makes a closure of the membrane energetically more favourable so that it occurs at an earlier stage of disk growth. As a result we could show that size and formation kinetics of vesicles in a surfactant mixture can be controlled in a systematic way by the charge conditions of the head groups of the surfactants involved. While this was demonstrated here for a model system, it can be expected to apply in general to similar surfactant mixtures and therefore be of general importance to the field of surfactant self-assembly.

Conflicts of interest

There are no conflicts to declare.

Data availability

The NSE data is available under **https://doi.ill.fr/10.5291/ILL-DATA.CRG-2637**. SANS data from ISIS is available *via* DOI: **https://doi.org/10.5286/ISIS.E.RB1810642**. SANS data from ILL is available under **https://doi.ill.fr/10.5291/ILL-DATA.9-11-1896**.

Supplementary information (SI): data and intermediate results of SANS, DLS and NSE analysis. See DOI: **https://doi.org/10.1039/d5sm00600g**.

Acknowledgements

Our thanks go to Jana Lutzki for experiments in preparation of the stopped-flow SANS beamtime. We would like to thank the ILL and ISIS for the allocation of beamtime and financial support regarding the associated travel expenses. Financial support from the BMBF Project No. 05K13KT1 is gratefully acknowledged.

References

1 R. Laughlin, *Colloids Surf., A*, 1997, **128**, 27–38.
2 V. Guida, *Adv. Colloid Interface Sci.*, 2010, **161**, 77–88.
3 R. G. Morris and A. J. McKane, *Phys. Rev. E*, 2011, **83**, 061151.
4 Y. Talmon, D. F. Evans and B. W. Ninham, *Science*, 1983, **221**, 1047–1048.
5 N. E. Gabriel and M. F. Roberts, *Biochemistry*, 1984, **23**, 4011–4015.
6 K. L. Herrington, E. W. Kaler, D. D. Miller, J. A. Zasadzinski and S. Chiruvolu, *J. Phys. Chem.*, 1993, **97**, 13792–13802.
7 R. Talhout and J. B. F. N. Engberts, *Langmuir*, 1997, **13**, 5001–5006.
8 J. D. Morgan, C. A. Johnson and E. W. Kaler, *Langmuir*, 1997, **13**, 6447–6451.
9 E. F. Marques, O. Regev, A. Khan, M. da Graca Miguel and B. Lindman, *J. Phys. Chem. B*, 1998, **102**, 6746–6758.
10 H.-P. Hentze, S. R. Raghavan, C. A. McKelvey and E. W. Kaler, *Langmuir*, 2003, **19**, 1069–1074.
11 J. Hao, H. Hoffmann and K. Horbaschek, *Langmuir*, 2001, **17**, 4151–4160.
12 H.-T. Jung, S. Y. Lee, E. W. Kaler, B. Coldren and J. A. Zasadzinski, *Proc. Natl. Acad. Sci. U. S. A.*, 2002, **99**, 15318–15322.
13 S. Schmölzer, D. Gräbner, M. Gradzielski and T. Narayanan, *Phys. Rev. Lett.*, 2002, **88**, 258301.
14 M. Bergström, *Langmuir*, 1996, **12**, 2454–2463.
15 M. Gradzielski, *J. Phys.: Condens. Matter*, 2003, **15**, R655.
16 S. Šegota and D. Težak, *Adv. Colloid Interface Sci.*, 2006, **121**, 51–75.
17 A. J. O'Connor, T. A. Hatton and A. Bose, *Langmuir*, 1997, **13**, 6931–6940.
18 Y. Xia, I. Goldmints, P. W. Johnson, T. A. Hatton and A. Bose, *Langmuir*, 2002, **18**, 3822–3828.
19 S. Bucak, B. H. Robinson and A. Fontana, *Langmuir*, 2002, **18**, 8288–8294.
20 T. M. Weiss, T. Narayanan and M. Gradzielski, *Langmuir*, 2008, **24**, 3759–3766.
21 I. Grillo, E. I. Kats and A. R. Muratov, *Langmuir*, 2003, **19**, 4573–4581.
22 W. Helfrich, *Phys. Lett. A*, 1974, **50**, 115–116.
23 A. Shioi and T. A. Hatton, *Langmuir*, 2002, **18**, 7341–7348.

24 J. Leng, S. Egelhaaf and M. Cates, *Biophys. J.*, 2003, **85**, 1624–1646.
25 K. Bressel, M. Muthig, S. Prévost, I. Grillo and M. Gradzielski, *Colloid Polym. Sci.*, 2010, **288**, 827–840.
26 T. M. Weiss, T. Narayanan, C. Wolf, M. Gradzielski, P. Panine, S. Finet and W. I. Helsby, *Phys. Rev. Lett.*, 2005, **94**, 038303.
27 K. Bressel, S. Prévost, M. Appavou, B. Tiersch, J. Koetz and M. Gradzielski, *Soft Matter*, 2011, **7**, 11232–11242.
28 T. Narayanan, M. Sztucki, T. Zinn, J. Kieffer, A. Homs-Puron, J. Gorini, P. van Vaerenbergh and P. Boesecke, *J. Appl. Crystallogr.*, 2022, **55**, 98–111.
29 K. Bressel, M. Muthig, S. Prévost, J. Gummel, T. Narayanan and M. Gradzielski, *ACS Nano*, 2012, **6**, 5858–5865.
30 P. Fromherz, *Chem. Phys. Lett.*, 1983, **94**, 259–266.
31 J. N. Israelachvili, D. J. Mitchell and B. W. Ninham, *J. Chem. Soc., Faraday Trans. II*, 1976, **72**, 1525–1568.
32 E. G. Kelley, P. D. Butler, R. Ashkar, R. Bradbury and M. Nagao, *Proc. Natl. Acad. Sci. U. S. A.*, 2020, **117**, 23365–23373.
33 A. Búcsi, J. Karlovská, M. Chovan, F. Devínsky and D. Uhríková, *Chem. Papers*, 2013, **68**, 842–846.
34 K. Bressel, PhD thesis, TU Berlin, 2014.
35 R. K. Heenan, S. E. Rogers, D. Turner, A. E. Terry, J. Treadgold and S. M. King, *Neutron News*, 2011, **22**, 19–21.
36 **https://www.isis.stfc.ac.uk**.
37 **https://www.mantidproject.org**.
38 LAMP, the Large Array Manipulation Program. **https://www.ill.eu/data_treat/lamp/the-lamp-book/**.
39 I. Grillo, *Soft Matter Characterization*, Springer, 2008, ch. 13, pp. 725–782.
40 **https://github.com/BAMresearch/dataMerge**.
41 B. Farago, P. Falus, I. Hoffmann, M. Gradzielski, F. Thomas and C. Gomez, *Neutron News*, 2015, **26**, 15–17.
42 A. G. Zilman and R. Granek, *Phys. Rev. Lett.*, 1996, **77**, 4788–4791.
43 R. Granek, I. Hoffmann, E. G. Kelley, M. Nagao, P. M. Vlahovska and A. Zilman, *Eur. Phys. J. E*, 2024, **47**, 12.
44 M. C. Watson, Y. Peng, Y. Zheng and F. L. H. Brown, *J. Chem. Phys.*, 2011, 135.
45 U. Seifert and S. A. Langer, *Europhys. Lett.*, 1993, **23**, 71–76.
46 W. Rawicz, K. Olbrich, T. McIntosh, D. Needham and E. Evans, *Biophys. J.*, 2000, **79**, 328–339.
47 S. Gupta, J. U. de Mel and G. J. Schneider, *Curr. Opin. Colloid Interface Sci.*, 2019, **42**, 121–136.
48 I. Hoffmann, *Front. Phys.*, 2021, **8**, 602.
49 E. Karatekin, O. Sandre, H. Guitouni, N. Borghi, P. Puech and F. Brochard-Wyart, *Biophys. J.*, 2003, **84**, 1734–1749.